J. Plasma Phys. (2022), *vol*. 88, 905880404
Published by Cambridge University Press

doi:10.1017/S0022377822000599

Picosecond snapshot imaging of electric fields induced on a cone guide target designed for fast ignition scenario

Binghe Shi[1], Akifumi Yogo[1,†], Kazuki Okamoto[1], Daniil Golovin[1], Seyed Reza Mirfayzi[2], Alessio Morace[1], Yasunobu Arikawa[1], Kohei Yamanoi[1], Yuki Abe[3], Masakatsu Murakami[1], Yanjun Gu[1], Kunioki Mima[1], Yasuhiko Sentoku[1], Mitsuo Nakai[1], Hiroyuki Nishimura[4], Hiroyuki Shiraga[1], Shinsuke Fujioka[1], Tomoyuki Johzaki[5], Akifumi Iwamoto[6], Hitoshi Sakagami[6] and Ryosuke Kodama[1]

[1]Institute of Laser Engineering, Osaka University, 2-6 Yamadaoka, Suita, Osaka 567-0871, Japan

[2]Tokamak Energy Ltd, 173 Brook Dr, Milton, Abingdon OX14 4SD, UK

[3]Graduate School of Engineering, Osaka University, Suita 567-0871, Japan

[4]Fukui University of Technology, Fukui 910-0028, Japan

[5]Graduate School of Advanced Science and Engineering, Hiroshima University, 1-4-1 Kagamiyama, Higashi Hiroshima 739-8527, Japan

[6]National Institute for Fusion Science, Toki, Gifu 509-5202, Japan

(Received 6 December 2021; revised 31 May 2022; accepted 10 June 2022)

In this study, we experimentally evaluate the ion transportation through a cone guide target, which accelerates ions up to MeV energies via target normal sheath acceleration, and transports them onto the position of imploding fuel in the fast ignition scenario of nuclear fusion. We measured the electric and magnetic fields (EM-fields) induced by return current streaming along the cone wall by proton radiography, and we report that the EM-fields are predominantly induced within a temporal window up to 30 ps after the laser injection. The magnitude of the electric field is maximized around 13 ps, reaching 4.0×10^{10}V m^{-1}, when the magnetic field is below 200 T. The present scheme provides insights on the EM-fields evaluation in the time region that is difficult to treat with simulations due to the computing resources.

Key words: intense particle beams, plasma devices

1. Introduction

The ion acceleration by high-intensity laser beam is a subject of interest for a wide range of applications, such as tumour treatment (Bulanov & Khoroshkov 2002), neutron generation (Mirfayzi *et al.* 2020; Mori *et al.* 2021; Yogo *et al.* 2021) and a driver

† Email address for correspondence: yogo-a@ile.osaka-u.ac.jp

beam for the fast ignition (FI) (Roth *et al.* 2001) used in inertial confinement fusion. The original concept of FI envisioned that the hot electrons produced by laser–fuel interaction work as the energy transport medium to ignite the deuterium–tritium fusion. The deuterium–tritium fuel is often attached with a hollow cone in order to effectively transport the laser light to the compressed core (Kodama *et al.* 2001; Azechi *et al.* 2009). In the electron-driven FI research, the driver beam of hot electrons have a large divergence angle of approximately 100° and some part of the hot electrons is scattered and absorbed by the guiding hollow cone, especially for a high-Z cone (Johzaki *et al.* 2008). To resolve this issue, some approaches were proposed. One of the most effective methods is to utilize an extremely strong magnetic field driven by a laser to constrain the divergence angle of hot electrons (Sakata *et al.* 2018; Matsuo *et al.* 2020).

On the other hand, a concept of the ion-driven FI (Roth *et al.* 2001; Borghesi *et al.* 2004) was proposed as an alternative to the electron-driven FI. It was shown in the simulation (Sakagami *et al.* 2016) that the core heating efficiency of an ion beam can be enhanced by 20 %–60 %, compared with the electron-driven FI (Borghesi *et al.* 2004; Sakagami *et al.* 2016). Honrubia *et al.* revealed by the simulation that the driver protons are collimated by the electric and magnetic fields (EM-fields) induced on the inner surface of the guide cone.

In general, the ions accelerated by high-intensity laser–plasma interactions, including target normal sheath acceleration, are in time scale of the order of femtoseconds to picoseconds, which is close to the laser pulse duration. This feature of laser-accelerated ions provides a unique probing tool for diagnosing EM-fields in highly transient plasma (Mackinnon *et al.* 2004), combining other features of laser-driven proton beams, such as the remarkable collimation, high cutoff energy and small transverse emittance. This technique, termed proton radiography (PR), has been used to measure the high-speed dynamics of EM-fields (Romagnani *et al.* 2008) driven by lasers.

During the high-intensity laser irradiation of the cadmium (Cd) foil of the cone guide target, fast electrons are accelerated to nearly the speed of light and escape from the laser focal spot into vacuum. This will lead to a positive electrostatic potential growing up around the laser focus spot (Zhu *et al.* 2015). This positive potential drags the background cold electrons to the focus spot to neutralize the electric charges. The stream of these electrons along the target surface makes a current, called the return current, and this return current will create strong EM-fields (Quinn *et al.* 2009). As for the cone guide target, we assume the return current would flow along the cone-wall surface and generate strong EM-fields around the cone wall which affects the propagation of ions throughout the gold cone.

In this paper, we experimentally study the ion transportation through a hollow gold cone, which is designed for ion-driven FI. We discuss the method to diagnose the EM-fields induced on the cone guide using the PR technique. We report the results of PR imaging in the time range of 1.5–38 ps after the laser injection, which is beyond the time region that can be accessed by particle-in-cell (PIC) simulations. With the assistance of particle tracing simulation, we evaluate the EM-fields and discuss the ion transportation through the cone guide targets.

2. Experiment

We measured the EM-fields with the PR method. The experiment was conducted on the LFEX laser at the Institute of Laser Engineering, Osaka University (Kawanaka *et al.* 2008). The experimental set-up is schematically shown in figure 1. In order to perform the PR imaging, we fabricated the cone guide target as shown in figure 1(*b*): we made a gold cone target having an opening angle of 45°, thickness of 7 μm and a length of 750 μm; the

https://doi.org/10.1017/S0022377822000599 Published online by Cambridge University Press

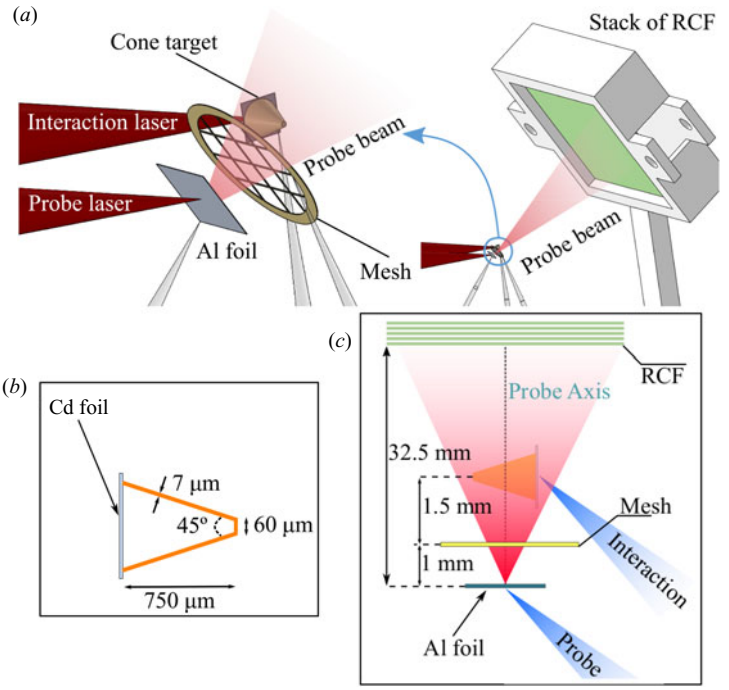

FIGURE 1. (*a*) The experimental set-up. (*b*) The design drawing of the cone target. (*c*) The top view of the experimental set-up.

cone was directly attached to the Cd foil. One of the laser beams was used as an interaction laser, which gave an on-target energy of 200 J with an intensity of 2×10^{18} W cm^{-2}. Another laser beam with on-target intensity approximately 6×10^{18} W cm^{-2} was used as the probe laser, and was focused onto a 10 μm Al foil to generate the proton beam with the cutoff energy of roughly 20 MeV for probing the interaction area. A 55 ps optical delay was set on the pump laser so as to envelop the entire interaction into the probe beam. The radiochromic films (RCF) (GAFChromic 2020*a*,*b*) were employed transverse to the probe beam as a proton detector. By stacking RCFs layer by layer, the proton deflection images resolved energetically. Since each RCF is related to a proton energy E_p by calculating the distance into the RCF stack where the Bragg peak occurs, the picosecond continuous observation of the evolution of EM-fields around the cone target was realized by calculating the time-of-flight of corresponding protons (Quinn *et al.* 2009). It is important to note that the proton accelerated from the Al foil has an angular distribution of 60°. Hence, EM-fields were measured along the probe axis from which the accelerated protons have no horizontal velocity component.

3. The results and analysis of the EM-fields measurements

The proton deflection images deposited on RCFs are shown in figure 2. Comparing the RCF images at different probe times, the evolution of the proton profile around the cone target is seen clearly. Since the flight trajectory of probe protons is deflected by the EM-fields around the cone target, the evolution of the proton profile is synchronous to the evolution of EM-fields around cone target. Around the cone walls in the images of $t = 8.7$, 13.1 and 20.5 ps, one can recognize mesh patterns, which are not perturbed by the EM-fields. This is attributed to the fact that the reduction of the proton density reveals

https://doi.org/10.1017/S0022377822000599 Published online by Cambridge University Press

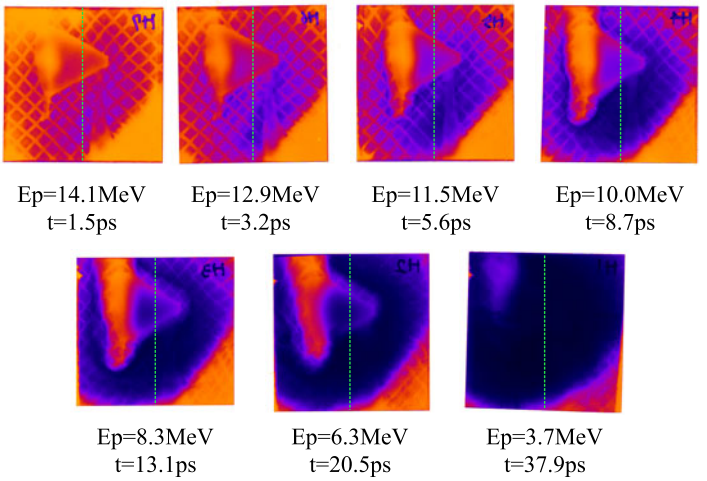

FIGURE 2. The results of RCF measurements. The green line marks the probe axis. The energies of protons predominantly stopped at the RCF layer are shown below the images. The time t indicates the relative time that the protons passed through the cone target after the laser irradiation onto the cone target. The inset shows the result with the glass stoke attached on the Cd foil, not on the tip of the cone.

the hidden images of the mesh printed by the passing through of higher-energy protons, as detected by deeper layers of RCFs ($t = 1.5$, 3.2 ps).

In the frame of $t = 5.6$ ps, one can see the image of the EM-field arriving at the bottom of the cone. In the next frame ($t = 8.7$ ps), the EM-field reaches the tip of the cone, indicating that the front of the EM-field moved along the distance of the cone wall (0.82 mm) within 3.2 ps. Then, the speed of the EM-fields' front is estimated to be $v_f \sim 0.9c$, where c is the speed of light in vacuum.

It is important to note that the EM-fields are induced predominantly in the temporal window of 15–30 ps, which is approximately 10 times longer than the laser pulse duration. It is experimentally found that the EM-field is induced by the return current, not by the hot electrons. The inset of figure 2 shows the RCF image measured when the glass stalk is attached to the Cd foil, not on the tip of the cone. In this case, the return current is generated only on the Cd foil, and the EM-fields were not induced on the cone wall. This is direct evidence that the EM-field is induced by the return current, not the hot electrons.

We performed a Monte Carlo simulation on the proton trajectory by a three dimensional particle tracing code, PRORAD (Wilks & Black 2017), in order to reproduce the PR images. Here, we set static electric ($\boldsymbol{E_d}$) and magnetic $\boldsymbol{B_r}$ fields, as shown in figure 3, for the each run of the Monte Carlo simulation, where the protons having same kinetic energy are generated from the source with a random divergence angle in the range of 0°–20°. The protons are traced one by one until the accumulation is obtained with sufficient statistics. Considering that the 10 MeV probe protons, for instance, pass through the typical thickness of the EM-fields (50 μm) within 1 ps, it is reasonable to assume that the EM-fields are static during the time that the probe protons pass through. Assuming that $\boldsymbol{E_d}$ is the radial outside-directed electric field around the cone surface, we set the strength of $\boldsymbol{E_d}$ by applying Gauss's law: $E_d = E_{\max}(l_c/l)$, $l \geqslant l_c$ and the continuity equation $I = 2\pi\epsilon_0 l_c v_f E_{\max}$. Here, $E_{\max}$ is the strength of the electric field at the cone outer surface, $l_c = 3.5$ μm is half of the cone-wall thickness and l represents the distance from any point outside to the centre of the cone wall. With the flow of return current inside the cone

https://doi.org/10.1017/S0022377822000599 Published online by Cambridge University Press

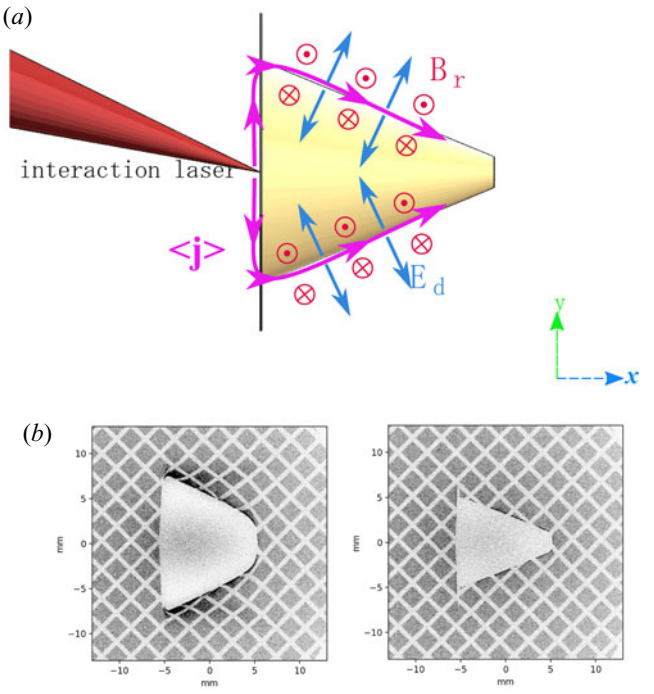

FIGURE 3. (*a*) The schematic diagram of electric field $\boldsymbol{E_d}$ and magnetic field $\boldsymbol{B_r}$ generated by the return current induced on the cone wall. (*b*) The results of particle tracing simulation assuming the EM-fields induced by the return current of 2.1 kA. The left-hand side shows the cone target only with electric field of 4.0×10^{10} V m^{-1}. The right-hand one shows the result assuming only the magnetic field of 120 T.

wall, an azimuthal magnetic field $\boldsymbol{B_r}$ is generated and its strength can be calculated using Ampere's law.

In general, it is quite difficult to distinguish the electric fields from the magnetic fields by using the images of the proton deflection. In our approach, we calculate the EM-fields separately in the PRORAD simulation and discuss which field is predominant in the present cone guide geometry. Figure 3(*b*) shows the PR images calculated separately for the electric (left-hand subpanel) and magnetic (right-hand subpanel) fields induced by assuming the return current of 2.1 kA inside the cone. While the proton image is drastically modified by the electric field of $E_{\max} = 4.0 \times 10^{10}$ V m^{-1}, the magnetic field (120 T) makes no significant change on the image. Also, Quinn *et al.* discussed (Quinn *et al.* 2009) that the proton deflection by the magnetic field is not significant as long as the magnetic field strength is smaller than 200 T. Hence, in this study we assume that the proton deflection by magnetic fields is negligible when the return current is of the order of 10^{10} V m^{-1}, and evaluate the electric fields induced on the cone guide from the PR images.

The simulated results by the PRORAD code are compared with the experimental PR images in figure 4(*a–d*). In the simulation, we adjusted the electric fields on the cone wall to find agreements with the width of the proton-deflected zone, shown as the dashed lines in figure 4(*b–d*). The electric fields on the cone wall are evaluated for $t = 8.7$, 13.1, 20.5 ps and shown in figure 4(*e*). Considering that there is a clear difference between the PR images for $t = 8.7$ ps (figure 4*b*) and $t = 13.1$ ps (figure 4*c*), the errors of the measured electric fields seems to be smaller than 50 %. As a result, we find that the electric field

https://doi.org/10.1017/S0022377822000599 Published online by Cambridge University Press

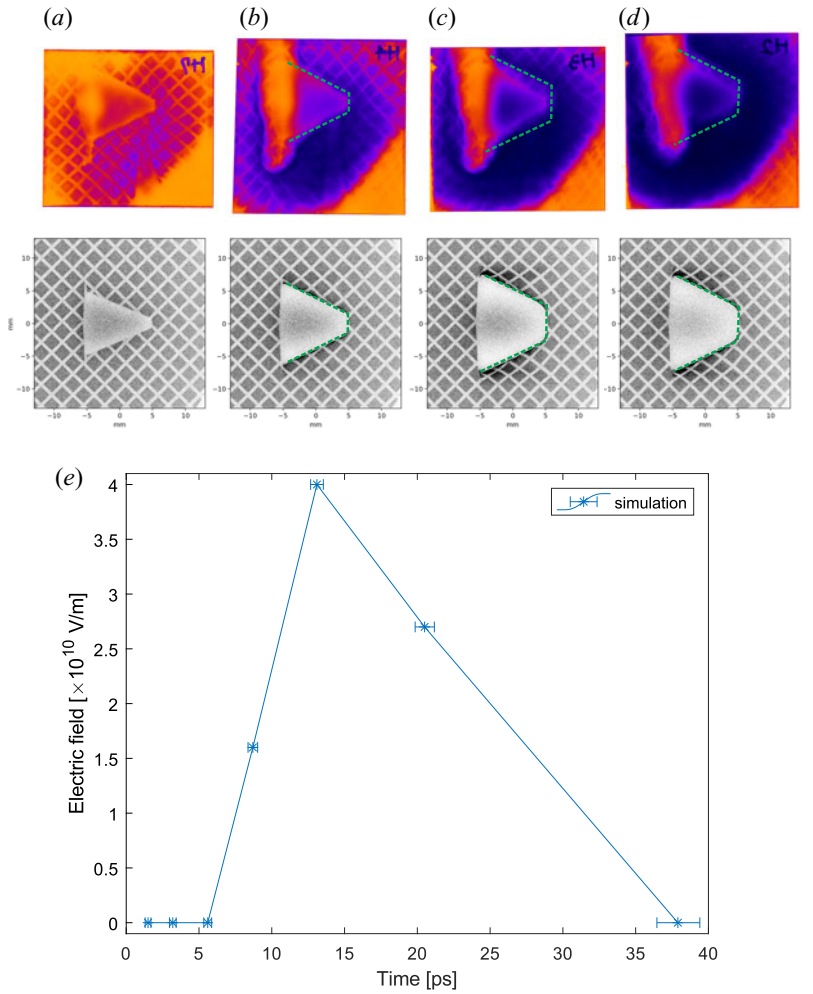

FIGURE 4. (*a–d*) Results of particle tracing simulation for the time (*a*) 1.5 ps; (*b*) 8.7 ps; (*c*) 13.1 ps; (*d*) 20.5 ps. (*e*) The maximum strength of the electric field (E_{max}) obtained for (*a–d*) as a function of the time.

reaches $E_{max} = 4.0 \times 10^{10}$ V m^{-1} at a maximum with $t = 13.1$ ps after the laser shot. The corresponding return current is estimated to be 2.1 kA, which generates the magnetic field around 120 T, which makes no significant change on the PR image, as shown in figure 3(*b*). Hence, the proton deflection on the PR images are attributed to the electric fields that reache $\sim 10^{10}$ V m^{-1} on the cone surface.

4. Two-dimensional PIC simulation

To discuss the evolution of the electric field by the interaction of an ultrahigh-intensity laser with the cone guide target, we performed two-dimensional PIC simulation using the EPOCH code (Arber *et al.* 2015). Considering the balance of computing resource consumption, the size of the cone target is scaled down to 25 % of the experiment, and the simulation was performed until $t = 1.5$ ps. The size of the simulation box was 250 μm × 210 μm and the incident laser pulse of $\lambda = 1.05$ μm wavelength, 6×10^{18} W cm^{-2} peak intensity, 1.5 ps duration and 12.5 μm spot diameter, normally incident with a cone

https://doi.org/10.1017/S0022377822000599 Published online by Cambridge University Press

guide target. Note the thickness of the Cd foil and gold cone remains consistent with the diagnostic experiment which are still 5 μm and 7 μm, respectively. The irradiated Cd foil target plasma extends over $0 \leqslant x \leqslant 5$ μm and the laser pulse shot from the left-hand side at $x = 0$, $y = 0$. Figure 5 shows the distribution of E_y, B_z and J_x (the components of electric field, magnetic field and current density along the coordinate system) at the time of $T = 1$ ps (figure 5*a*,*c*,*e*) and $T = 1.5$ ps (figure 5*b*,*f*,*e*). It is obviously seen that the front of J_x moves towards the cone tip. This fact is the evidence that the current is induced as a return current, not as the flow of hot electrons generated from the focal spot. The speed of J_x front is estimated to be 0.85–0.9*c*, which is almost the same as the speed of the EM-fields measured with the PR images discussed in § 3. The J_x flows along the inner and outer surfaces of the cone wall and simultaneously induce the electric field and magnetic field in the outwards and parallel direction of the cone wall, respectively. The directions of E_y and B_z are in agreement with the direction of EM-fields shown in figure 3(*a*).

5. Discussion

Combining the results obtained with the EM-fields' diagnostic experiment and simulations, we reported that the EM-fields are generated with a temporal window of 8–20 ps after the laser incidence. In this section, we discuss the relationship between the EM-fields' generation around the cone, and ion propagation. We measured the ion transportation by using the targets shown in figure 6. Note the cone length is 1 mm, which is 33 % longer than those used in the PR measurements. The Cd foil was placed on a bridge of glass stokes (figure 6*b*), the materials of which are the same as with the stoke attached on the cone tip. The glass bridge is expected to work as the pathway of the return current. To measure the accelerated ion energies, a Thomson parabola (TP) ion analyser (Tosaki *et al.* 2017; Golovin *et al.* 2021) was placed on the laser incident axis at a distance of 0.95 m from the target. The ion energy spectra are shown in figure 6(*d*). For the reference shot using the 5 μm Cd foil without the cone, the maximum proton and deuteron are accelerated up to 30.5 MeV and 8.8 MeV n^{-1} (17.6 MeV in total), respectively, with the laser intensity of 1.1×10^{19} W cm^{-2}. The spectra of protons and deuterons were also observed in Mirfayzi *et al.* (2020), Mori *et al.* (2021) and Yogo *et al.* (2021), with the mechanism of ion acceleration discussed in detail in Yogo *et al.* (2017) and Iwata *et al.* (2017). For the cone guide target, the maximum energy of protons and deuterons are decreased: 12.9 MeV for protons and 6.7 MeV n^{-1} (13.4 MeV in total) for deuterons. Especially, the energy decrease seen for the protons is severe.

Considering the geometric size of the cone guide target, which was shown in figure 6(c), the flight time for a 30 MeV proton to travel from the Cd foil to the tip of the cone is approximately 13 ps. For the 10 MeV deuterons, the flight time is approximately 23 ps. The arrival time (around 13 ps) of protons at the cone tip is in agreement with the time that the EM-fields are predominantly induced. Hence, the protons are strongly influenced by the EM-fields during the transport process. On the other hand, since the arrival time for deuterons (>23 ps) is longer than the existing time of the EM-fields. This scenario indicates the reason why the protons were not measured at the position of the TP ion analyser, as shown in figure 6.

The EM-fields affect the ion propagation in two different ways (Honrubia, Morace & Murakami 2017) as follows: (i) the electric field induced in the perpendicular direction to the cone surface pushes and focuses the ions towards the centre axis of the cone; (ii) the magnetic field induced on the cone wall defocuses the ions, on the contrary. In our experimental condition with the laser intensity around 10^{18} W cm^{-2}, we have experimentally found that the effect of the electric field is more predominant than the magnetic field for the ion transportation. Hence, it is reasonable to consider that the

https://doi.org/10.1017/S0022377822000599 Published online by Cambridge University Press

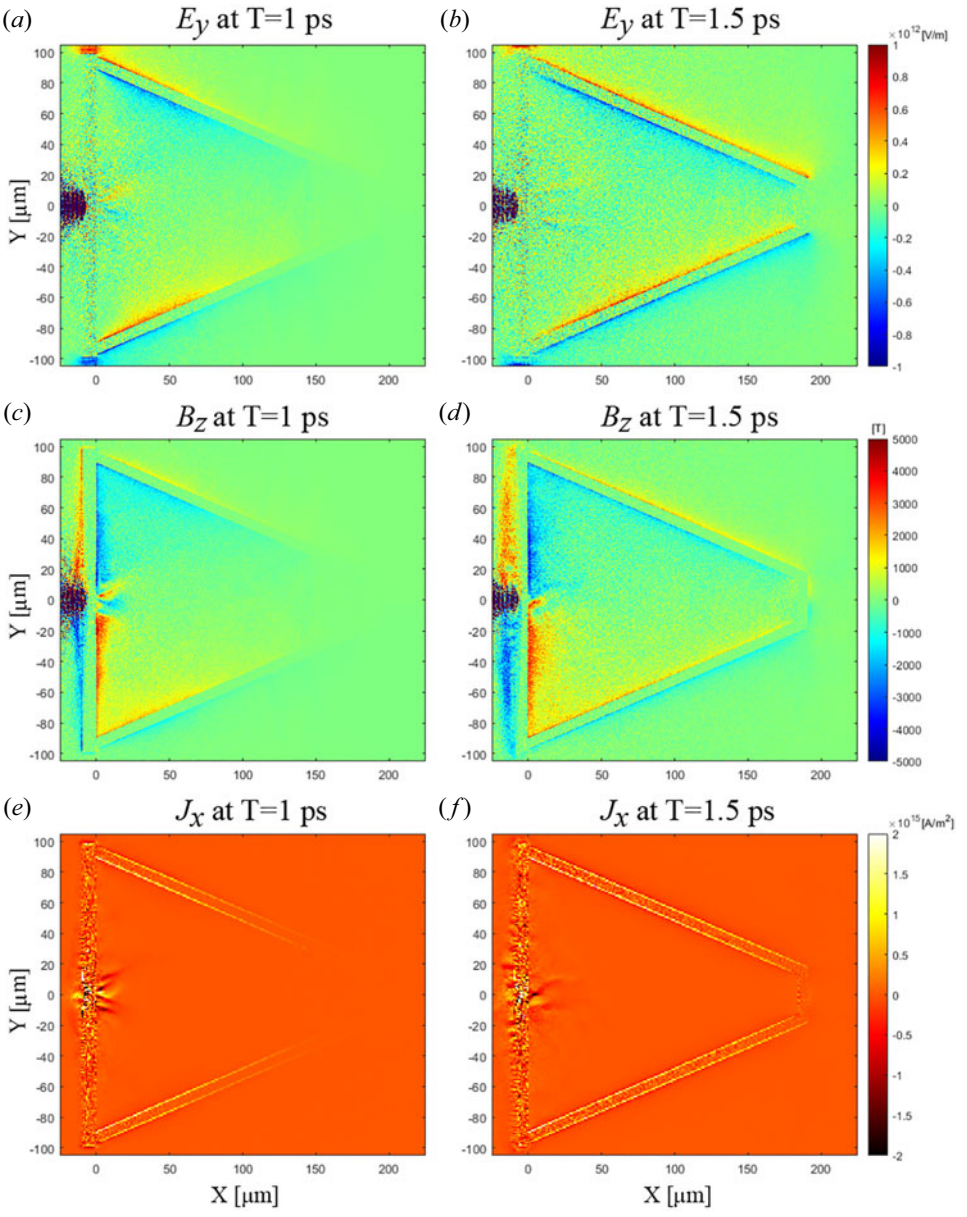

FIGURE 5. The results of PIC simulation showing the of electric field (E_y), magnetic field (B_z) and current density (J_x) along the target surface at the time $T = 1$ ps (a,c,e) and $T = 1.5$ ps (b,d,f).

trajectories of the higher-energy protons (15–30 MeV) were bent by the electric fields induced on the cone wall and focused at the exit of the cone, according to the scenario (i) mentioned above. As a result, the protons were again diverged after passing through the focal point, and not measured by the TP far from the target.

At the laser intensity around 10^{20} W cm^{-2} typically used for the ion-driven FI, the return currents should be much higher and the magnetic field may play an important role on the

https://doi.org/10.1017/S0022377822000599 Published online by Cambridge University Press

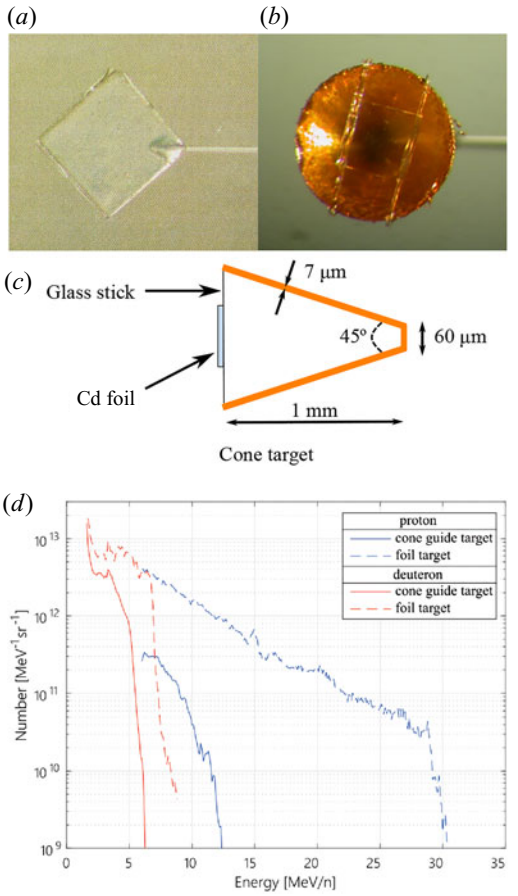

FIGURE 6. (*a*) Photograph of normal Cd foil target. (*b*) Photograph of cone guide Cd foil target. (*c*) Drawing of the cone guide target's structure in detail. (*d*) The ions energy spectrum obtained by laser-axis TP for cone guide target and foil target. The results of cone guide target and foil target are drawn in solid and dashed lines, respectively. Blue and red lines represent proton and deuteron.

ion transportation. The PR method in this study will provide a powerful tool for further investigations at high laser intensities scalable to the FI conditions.

6. Conclusion

In this work, we demonstrated the 'snapshot' imaging of the EM-fields generated around the cone guide target designed for fusion FI research. With the help of the PR technique and particle tracing simulation, we measured the temporal evolution of the EM-fields. As a result, we found that the electric field reached 4.0×10^{10} V m^{-1} around 15 ps after the laser shot, while the magnetic field did not exceed 120 T. It should be emphasized that the EM-fields were evaluated experimentally in the time range that is difficult to simulate with PIC codes due to the limit of computing resources. At this stage, our scheme of diagnosing the EM-fields will lead to the new design of cone guide targets, which are scalable to the FI conditions. In addition, the PR scheme provides a powerful tool of high-speed diagnostics in the field of high-energy-density physics.

https://doi.org/10.1017/S0022377822000599 Published online by Cambridge University Press

Acknowledgements

Editor V. Malka thanks the referees for their advice in evaluating this article.

Funding

The authors thank the technical support staff of ILE and the Cyber Media Center at Osaka University for assistance with the laser operation, target fabrication and plasma diagnostics. This study was performed under the Collaboration Research Program between the National Institute for Fusion Science and the Institute of Laser Engineering at Osaka University (A.Y., no. NIFS15KUGK096 and A.Y., no.NIFS18KUGK119) and by the Japanese Ministry of Education, Science, Sports and Culture through Grants-in-Aid, KAKENHI (M.M., grant no. 21H004454 and A.Y., grant no. 22H02007), Bilateral Program for Supporting International Joint Research by JSPS, (A.Y., grant no. JSJSBP120209922 and M.M., grant no. JSJSBP120204811).

Declaration of interests

The authors report no conflict of interest.

REFERENCES

Arber, T., Bennett, K., Brady, C., Lawrence-Douglas, A., Ramsay, M., Sircombe, N., Gillies, P., Evans, R., Schmitz, H., Bell, A., *et al.* 2015 Contemporary particle-in-cell approach to laser-plasma modelling. *Plasma Phys. Control. Fusion* **57** (11), 113001.

Azechi, H., Mima, K., Fujimoto, Y., Fujioka, S., Homma, H., Isobe, M., Iwamoto, A., Jitsuno, T., Johzaki, T., Kodama, R., *et al.* 2009 Plasma physics and laser development for the fast-ignition realization experiment (FIREX) project. *Nucl. Fusion* **49** (10), 104024.

Borghesi, M., Mackinnon, A.J., Campbell, D.H., Hicks, D.G., Kar, S., Patel, P.K., Price, D., Romagnani, L., Schiavi, A. & Willi, O. 2004 Multi-mev proton source investigations in ultraintense laser-foil interactions. *Phys. Rev. Lett*. **92**, 055003.

Bulanov, S. & Khoroshkov, V. 2002 Feasibility of using laser ion accelerators in proton therapy. *Plasma Phys. Rep*. **28** (5), 453–456.

GAFChromic 2020*a* Data sheet of hd-v2. http://www.gafchromic.com/documents/gafchromic-hdv2.pdf.

GAFChromic 2020*b* Data sheet of md-v3. http://www.gafchromic.com/documents/gafchromic-mdv3.pdf.

Golovin, D., Mirfayzi, S., Shokita, S., Abe, Y., Lan, Z., Arikawa, Y., Morace, A., Pikuz, T. & Yogo, A. 2021 Calibration of imaging plates sensitivity to high energy photons and ions for laser-plasma interaction sources. *J. Instrum*. **16** (02), T02005–T02005.

Honrubia, J., Morace, A. & Murakami, M. 2017 On intense proton beam generation and transport in hollow cones. *Matter Radiat. Extremes* **2** (1), 28–36, special Issue on Laser Fusion (I).

Iwata, N., Mima, K., Sentoku, Y., Yogo, A., Nagatomo, H., Nishimura, H. & Azechi, H. 2017 Fast ion acceleration in a foil plasma heated by a multi-picosecond high intensity laser. *Phys. Plasmas* **24** (7), 073111.

Johzaki, T., Sentoku, Y., Nagatomo, H., Sakagami, H., Nakao, Y. & Mima, K. 2008 Core heating properties in FIREX-i—influence of cone tip. *Plasma Phys. Control. Fusion* **51** (1), 014002.

Kawanaka, J., Miyanaga, N., Azechi, H., Kanabe, T., Jitsuno, T., Kondo, K., Fujimoto, Y., Morio, N., Matsuo, S., Kawakami, Y., *et al.* 2008 3.1-kJ chirped-pulse power amplification in the LFEX laser. *J. Phys.: Conf. Ser*. **112** (3), 032006.

Kodama, R., Norreys, P.A., Mima, K., Dangor, A.E., Evans, R.G., Fujita, H., Kitagawa, Y., Krushelnick, K., Miyakoshi, T., Miyanaga, N., *et al.* 2001 Fast heating of ultrahigh-density plasma as a step towards laser fusion ignition. *Nature* **412** (6849), 798–802.

Mackinnon, A., Patel, P., Town, R., Edwards, M., Phillips, T., Lerner, S., Price, D., Hicks, D., Key, M., Hatchett, S., *et al.* 2004 Proton radiography as an electromagnetic field and density perturbation diagnostic. *Rev. Sci. Instrum*. **75** (10), 3531–3536.

MATSUO, K., HIGASHI, N., IWATA, N., SAKATA, S., LEE, S., JOHZAKI, T., SAWADA, H., IWASA, Y., LAW, K.F.F., MORITA, H., *et al.* 2020 Petapascal pressure driven by fast isochoric heating with a multipicosecond intense laser pulse. *Phys. Rev. Lett*. **124**, 035001.

MIRFAYZI, S., YOGO, A., LAN, Z., ISHIMOTO, T., IWAMOTO, A., NAGATA, M., NAKAI, M., ARIKAWA, Y., ABE, Y., GOLOVIN, D., *et al.* 2020 Proof-of-principle experiment for laser-driven cold neutron source. *Sci. Rep*. **10** (1), 1–8.

MORI, T., YOGO, A., HAYAKAWA, T., MIRFAYZI, S.R., LAN, Z., ABE, Y., ARIKAWA, Y., GOLOVIN, D., WEI, T., HONOKI, Y., *et al.* 2021 Direct evaluation of high neutron density environment using (n, 2n) reaction induced by laser-driven neutron source. *Phys. Rev.* C **104**, 015808.

QUINN, K., WILSON, P., CECCHETTI, C., RAMAKRISHNA, B., ROMAGNANI, L., SARRI, G., LANCIA, L., FUCHS, J., PIPAHL, A., TONCIAN, T., *et al.* 2009 Laser-driven ultrafast field propagation on solid surfaces. *Phys. Rev. Lett*. **102** (19), 194801.

ROMAGNANI, L., BORGHESI, M., CECCHETTI, C., KAR, S., ANTICI, P., AUDEBERT, P., BANDHOUPADJAY, S., CECCHERINI, F., COWAN, T., FUCHS, J., *et al.* 2008 Proton probing measurement of electric and magnetic fields generated by ns and ps laser-matter interactions. *Laser Part. Beams* **26** (2), 241.

ROTH, M., COWAN, T.E., KEY, M.H., HATCHETT, S.P., BROWN, C., FOUNTAIN, W., JOHNSON, J., PENNINGTON, D.M., SNAVELY, R.A., WILKS, S.C., *et al.* 2001 Fast ignition by intense laser-accelerated proton beams. *Phys. Rev. Lett*. **86**, 436–439.

SAKAGAMI, H., JOHZAKI, T., SUNAHARA, A. & NAGATOMO, H. 2016 Integrated simulations for ion beam assisted fast ignition. *J. Phys.: Conf. Ser*. **688**, 012096.

SAKATA, S., LEE, S., MORITA, H., JOHZAKI, T., SAWADA, H., IWASA, Y., MATSUO, K., LAW, K.F.F., YAO, A., HATA, M., *et al.* 2018 Magnetized fast isochoric laser heating for efficient creation of ultra-high-energy-density states. *Nat. Commun*. **9** (1), 3937.

TOSAKI, S., YOGO, A., KOGA, K., OKAMOTO, K., SHOKITA, S., MORACE, A., ARIKAWA, Y., FUJIOKA, S., NAKAI, M., SHIRAGA, H., *et al.* 2017 Evaluation of laser-driven ion energies for fusion fast-ignition research. *Prog. Theor. Exp. Phys*. **2017** (10), 103J01.

WILKS, S. & BLACK, M. 2017 Prorad code webpage. https://github.com/LLNL/prorad.

YOGO, A., MIMA, K., IWATA, N., TOSAKI, S., MORACE, A., ARIKAWA, Y., FUJIOKA, S., JOHZAKI, T., SENTOKU, Y., NISHIMURA, H., *et al.* 2017 Boosting laser-ion acceleration with multi-picosecond pulses. *Sci. Rep*. **7** (1), 1–10.

YOGO, A., MIRFAYZI, S.R., ARIKAWA, Y., ABE, Y., WEI, T., MORI, T., LAN, Z., HOONOKI, Y., GOLOVIN, D.O., KOGA, K., *et al.* 2021 Single shot radiography by a bright source of laser-driven thermal neutrons and x-rays. *Appl. Phys. Express* **14** (10), 106001.

ZHU, B.J., LI, Y.T., YUAN, D.W., LI, Y.F., LI, F., LIAO, G.Q., ZHAO, J.R., ZHONG, J.Y., XUE, F.B., HE, S.K., *et al.* 2015 Strong magnetic fields generated with a simple open-ended coil irradiated by high power laser pulses. *Appl. Phys. Lett*. **107** (26), 261903.